Geomechanics and Engineering, *Vol. 19, No. 5 (2019) 407-420*
DOI: https://doi.org/10.12989/gae.2019.19.5.407

Influence of structure-soil-structure interaction on foundation behavior for two adjacent structures: Geo-centrifuge experiment

Van-Linh Ngo[1a], Jae-Min Kim[2b] and Changho Lee*[3]

[1]*Department of Civil and Environmental Engineering, Chonnam National University, Yeosu 550-749, Korea*
[2]*Department of Civil Engineering, Chonnam National University, Gwangju 500-757, Korea*
[3]*Department of Marine and Civil Engineering, Chonnam National University, Yeosu 550-749, Korea*

(Received July 11, 2019, Revised November 14, 2019, Accepted November 18, 2019)

Abstract. This paper illustrates the results of a series of seismic geotechnical centrifuge experiments to explore dynamic structure-soil-structure interaction (SSSI) of two structures (named S1 and S2) installed on ground surface. A dense homogeneous ground is prepared in an equivalent shear beam (ESB) container. Two structural models are designed to elicit soil-foundation-structure interaction (SFSI) with different masses, heights, and dynamic characteristics. Five experimental tests are carried out for: (1) two reference responses of the two structures and (2) the response of two structures closely located at three ranges of distance. It is found that differential settlements of both structures increase and the smaller structure (S2) inversely rotates out of the other (S1) when they interact with each other. S2 structure experiences less settlement and uplift when at a close distance to the S1 structure. Furthermore, the S1 structure, which is larger one, shows a larger rocking and a smaller sliding response due to the SSSI effects, while S2 structure tends to slide more than that in the reference test, which is illustrated by an increase in sliding response and rocking stiffness as well as a decrease in moment-to-shear ratio (M/H·L) of the S2 structure.

Keywords: structure-soil-structure interaction; over-turning moment; base-shear force; rocking stiffness; moment-to-shear ratio

1. Introduction

It is widely known that dynamic response of a structure during earthquake is considerably affected by a soil-foundation-structure interaction (SFSI). Therefore, in modern seismic design codes, kinematic and inertial interaction effects were included in accessing a structure response so to consider the effect of SFSI (ASCE 2017, FEMA 2005). Furthermore, SFSI induces deformations of foundation includes rocking, sliding, and settling behaviors under seismic loading (Fatahi *et al.* 2014, Gajan and Kutter 2009b, Gajan *et al.* 2005, Kim *et al.* 2015, Kwon 2012, Trombetta *et al.* 2013). These foundation behaviors could not only reduce the structure response through rocking and sliding damping (Anastasopoulos *et al.* 2012, Drosos *et al.* 2012) but also mobilize ultimate bearing capacities of foundation (FEMA 2005, Gazetas *et al.* 2013). Therefore, several experimental studies have been performed to reveal rocking mechanism during earthquake and seismic loading. By conducting experiments using centrifuge models with various soil conditions, foundation dimensions, structure characteristics, and loading types, some studies observed that the moment-to-shear ratio (M/(H·L)) is one of the parameters whose effects control not only the rocking and sliding behaviors of the footing but modifications in the mobilization of the bearing capacity under couple vertical, horizontal, and moment loadings (Gajan and Kutter 2008, 2009b, Gajan *et al.* 2005). Also, degradation of rocking stiffness was found to be a power function of the rocking angle. Drosos *et al.* (2012), Gajan and Kutter (2008), and Ko *et al.* (2018) concluded that the vertical safety factor (FS_V), which is proportional to critical contact area ratio of the foundation (A/A_c, where A is foundation area and A_c is critical contact area between foundation and soil at ultimate condition of rocking structure) is a key parameter to decide whether the foundation uplifts or settles in response to rocking. More also, they indicated that seismic acceleration of the structure could be reduced by the uplifting and nonlinear rocking response of the foundation during an earthquake. By performing geo-centrifuge tests for structures with various natural frequencies, Kim *et al.* (2015) showed a reduction in the seismic response of a structure with a rocking foundation in comparison to a fixed-base structure. They also concluded that the effects of foundation rocking on structure response during an earthquake is undeniable and as a result, should not be ignored during an SFSI analysis.

Recently, structures are built close to each other in many cities and since two or more structures affect each other during an earthquake, a number of researches have been conducted to investigate the phenomenon of structure-soil-structure interaction (SSSI) (Aldaikh *et al.* 2015, Lee and Wesley 1973, Lou *et al.* 2011, Trombetta *et al.* 2014) or dynamic cross interaction (DCI) (Kitada *et al.* 1999, Kobori

*Corresponding author, Associate Professor
E-mail: changho@jnu.ac.kr
[a]Graduate Student
[b]Professor

http://www.techno-press.org/?journal=gae&subpage=7
ISSN: 2005-307X (Print), 2092-6219 (Online)

et al. 1973) with the hope of guiding engineers to avoid the hazards of unforeseen SSSI effects. A detrimental SSSI effect was observed on the response of structure which is shorter or lighter when placed adjacent to a taller or more massive structure (Aldaikh *et al.* 2015, Alexander *et al.* 2013, Chen *et al.* 1997, Kitada *et al.* 1999, Ogut 2017, Trombetta *et al.* 2014). Also, when the distance between structures is smaller than the foundations width, SSSI effects have been found to be more momentous (Aldaikh *et al.* 2015, Lee and Wesley 1973). The rocking restriction condition from a more massive structure to foundation of a lighter structure during earthquake when the two structures located close to each other because a reduction in permanent settlement of less massive structure at foundation near more massive structure, that results in the less massive structure rotated away the more massive structure (Mason *et al.* 2013). The rotation of the structure away from the adjacent structure were also reported when two structures were located at close distance between them base on a centrifuge experiment (Knappett *et al.* 2015). Furthermore, several researches concluded that the coupled rocking stiffness between structures modified the response of structure compared to that of an isolated structure. When structures are located close to each other, the modification of foundation response and rocking restriction between structures could change the structure respond during earthquake, and therefore, they play an important role in SSSI effects (Aldaikh *et al.* 2016, Aldaikh *et al.* 2018, Alexander *et al.* 2013). However, there is limited research to reveal the foundation behaviors (i.e., footing settlement and rotation) under SSSI effects (Knappett *et al.* 2015), especially for mat foundations with changing distances between structures.

In this study, five centrifuge experiments were performed to investigate the SSSI effects between two structures and its implication on the behavior of each foundation. A homogeneous ground was prepared by using a dense sand. Two single-degree-of-freedom (SDOF) structures that were made of aluminum were used, and each had different masses, heights, and structural dynamic characteristics. Soil-foundation responses, including foundation loads, rocking, and sliding were explored during an earthquake acceleration created by an in-flight earthquake simulator.

2. Geo-centrifuge experimental program

Modelling in the geo-centrifuge is one of the most effective ways to simulate SFSI problems during an earthquake, because it allows for the accurate duplication of principal dynamic properties of soil, including the shear strength, shear modulus, and damping (Cho *et al.* 2018; Ha *et al.* 2014). By increasing the centrifugal acceleration to N times, the self-weight stresses and the dimension of a small model could correspondingly be enlarged to N times following the centrifuge scaling law (Schofield 1980).

2.1 Design of soil-structure systems

The centrifugal experiments were carried out at KOCED

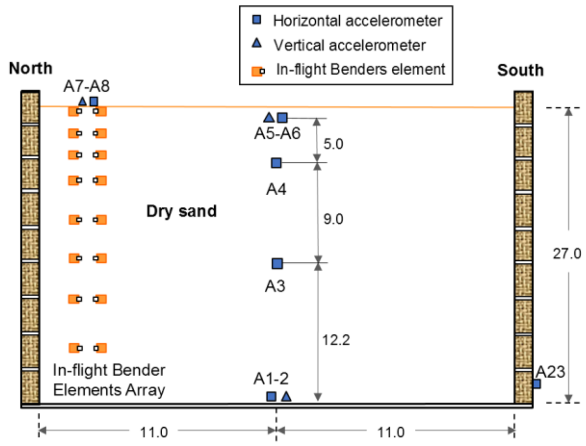

Fig. 1 Soil model with dry sand and installation of accelerometers, and in-flight bender element array to measure shear wave velocity profile. Unit in the Figure is meter

Table 1 Dimensionless parameters indicating SFSI and estimated values for S1 and S2 structures

Parameter	Range to enhance SFSI	Values for S1	Values for S2
$\frac{h_{eff}}{V_{s,FF}\ T}$	> 0.2	0.24	0.21
$\frac{h_{eff}}{r_\theta}$	> 0.1, < 4.0	3.15	2.95
$\frac{m_{st}}{\rho_s \pi r_e^2 h_{eff}}$	> 0.15	0.18	0.17
$\frac{D_f}{r_e}$	< 0.25	0.0	0.0
$\frac{m_{fnd}}{m_{str}}$	Minimize	0.97	1.03
$\frac{B}{2h_{eff}}$	Minimize	0.28	0.33

Note: h_{eff} = structure effective height; $V_{s,FF}$ = soil shear wave velocity at free-field; T = structure fixed-base period; m_{st} = structure mass; ρ_s = soil mass density; r_e = foundation equivalent sliding radius; D_f = foundation embedded depth; m_{fnd} = foundation mass; B = foundation width in shaking direction.

Geo-centrifuge Center, KAIST, South Korea, with a 5 m radius centrifuge machine at 45 *g* centrifugal acceleration. An equivalent shear beam (ESB) box was used to reduce boundary effects on the dynamic response of soil and structure (Lee *et al.* 2013). The ESB box has inner width and length of 490 mm each, and height dimensions of 630 mm.

A poorly-graded sand was used with an air-pluviation method to create a homogeneous ground with a thickness of 27 m at prototype scale in the ESB box as shown in Fig. 1. The soil used in this study has the following fundamental

Structures	S1	S2
Dimensions (m)	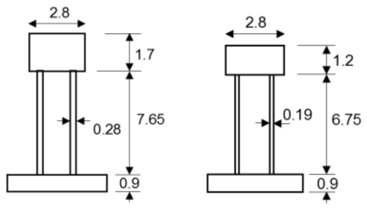	
Foundation parameters		
Length × width × thickness = L×B×T (m)	5.2×5.2×0.9	4.1×5.2×0.9
Sliding equivalent radius, $r_e = \sqrt{BL/\pi}$ (m)	2.95	2.55
Rocking equivalent radius, $r_\theta = \sqrt[4]{4I_f/\pi}$ (m)	2.98	2.80
Foundation mass at 1g, m_{fnd} (kg)	0.739	0.509
Structure parameters		
f_n at 45g, (Hz)	2.19	1.82
T at 45g, (sec)	0.46	0.54
Effective height, h_{eff} (m)	9.4	8.25
Structural mass at 1g, m_{st} (kg)	0.757	0.494
Sliding frequency, f_S (Hz)	5.89	6.72
Rocking frequency, f_R (Hz)	2.36	2.95

Note: I_f = moment of inertia of foundation;

Fig. 2 Characteristics of S1 and S2 structures.

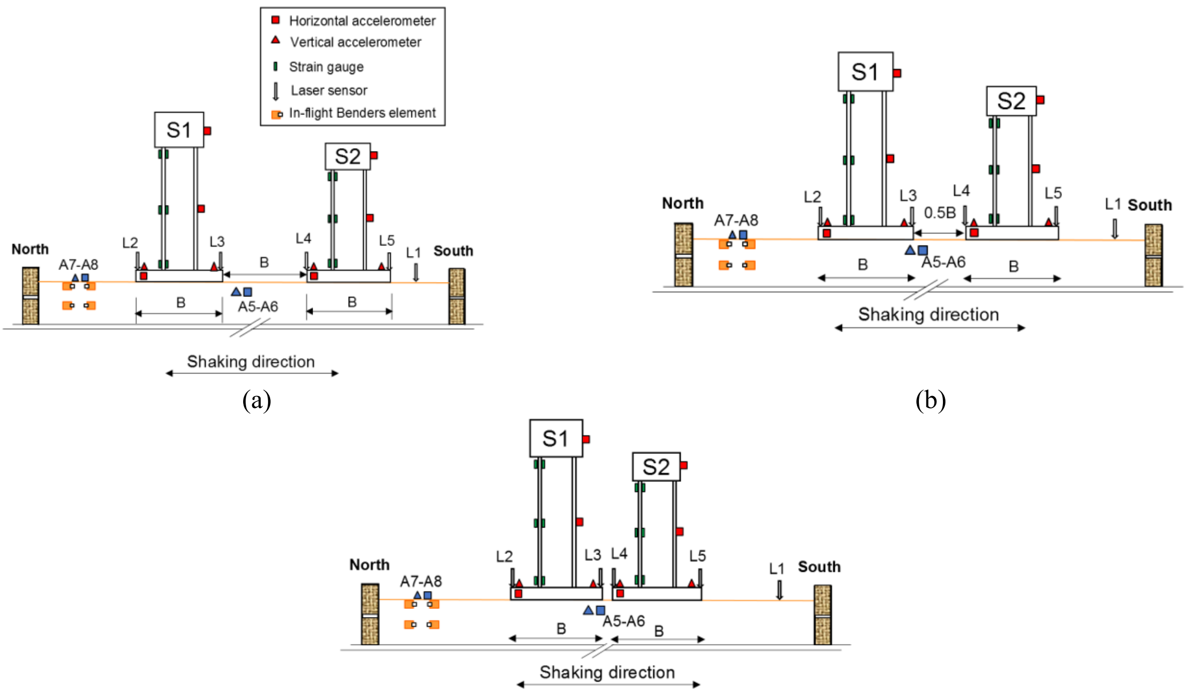

Fig. 3 Layout of centrifuge tests at various distances between S1 and S2 structures: (a) B distance; (b) 0.5B distance; and (c) 0.03B distance. B is width of the two structures.

characteristics: specific gravity (G_s) of 2.65; median particle size (D_{50}) of 0.237 mm; coefficient of uniformity (C_u) of 1.60; maximum (e_{max}) and minimum void ratios (e_{min}) of 1.137 and 0.616, respectively. The soil ground was prepared with a relative density (D_r) of approximately 80 % that corresponds to the dry unit weight of the soil of 15.12 kN/m^3. Critical state friction angle (ϕ'_{cs}) of the sand was found to be 36.6° by performing tri-axial compression test on specimen with the same D_r. An array of bender elements was installed to measure free-field shear wave velocity ($V_{s,FF}$ = 95 m/s) of ground and profile of in-flight shear wave velocity (V_s). Based on measured V_s and the ground thickness, the site fundamental frequency (f_{site}) was calculated to be approximately 2.03 Hz.

Aluminum was used to construct two single-degree-of-freedom (SDOF) structures, named S1 and S2 with different masses and heights. Fig. 2 shows dimensions of the two structures. The S1 structure has a square shaped foundation with the dimensions (B×L) of 5.22×5.22 m (B and L are width and length of foundation, respectively). The S2 structure has a rectangular shaped foundation with a similar width of S1, while the length, which is perpendicular to the shaking direction, was reduced to 4.12 m. Also, S1 is more massive than the S2 structure, with a mass ratio between the two structures ($\psi_{12} = m_{S1}/m_{S2}$) of 1.5 to expect high rocking restriction from S1 to S2 structure (Mason *et al.* 2013). Since S1 structure has a thicker wall than the S2 structure, despite having more height, S1 has a higher fixed-base frequency (f_n) than S2. The f_n of each structure was defined by performing an impact hammer test on the small-scale model, and with aid of the scaling laws (Schofield 1980), it was calculated to be 2.19 and 1.82 Hz for the S1 and S2 structures, respectively. The two structures were also designed with underlining SFSI in centrifugal experiments by: (1) approximately matching natural frequencies of structures with the site fundamental frequency (f_{site}), which was about 2 Hz; and (2) considering dimensionless parameters with emphasis on SFSI effects (Trombetta *et al.* 2014) as listed in Table 1. To define these dimensionless parameters, the effective height (h_{eff}) of SDOF structure needs to be found by considering massless wall. The structure mass (m_{st}) was firstly defined based on the mass of the roof (m_r) and mass of the walls (m_w), then h_{eff} was estimated from the wall stiffness (E_wI_w) and the fixed-base frequency (f_n) as (Beards 1996):

$$m_{st} = m_r + \frac{33}{140}m_w,\ f_n = \frac{1}{2\pi}\sqrt{\frac{3E_wI_w}{\left(m_r+\frac{33}{140}m_w\right)h_{eff}^3}} \tag{1}$$

The h_{eff} was calculated to be 9.4 m and 8.25 m for the S1 and S2 structures, respectively.

Foundation characteristics including the mass (m_{fnd}), equivalent foundation radius for sliding response (r_e), and foundation equivalent radius for rocking response (r_θ) were defined and listed in Fig. 2. The natural sliding frequencies (f_S) and rocking frequency (f_R) of the foundations on an elastic half-space were defined from the shear modulus of soil (G) beneath the structure, the structure mass (m), the foundation equivalent sliding radius (r_e), and the structural mass moment of inertia taken to center of foundation (I_o) as (Gazetas 1991, Park *et al.* 2017):

$$f_S = \frac{1}{2\pi}\sqrt{\frac{k_S}{m}} = \frac{1}{2\pi}\sqrt{\frac{9Gr_e}{m(2-\vartheta)}} \tag{2}$$

$$f_R = \frac{1}{2\pi}\sqrt{\frac{k_R}{m}} = \frac{1}{2\pi}\sqrt{\frac{8G(r_\theta)^3}{3I_o}} \tag{3}$$

f_S and f_R were calculated to be 5.89 Hz and 2.36 Hz for S1, and 6.72 and 2.95 for S2 structure, respectively.

Bearing capacity ratio (q_c/q) was defined based on a bearing stress (q) and a bearing capacity (q_c). q/q_c values for both structures were approximately designated as 0.05, which corresponding to vertical safety of factor (FS_v) of 19.6 for S1 and 22.5 for S2, for two reasons: (1) to increase the rocking-uplifting behavior of the structures (Drosos *et al.* 2012); and thus, (2) to reduce the soil densification beneath foundation when the seismic loading was applied.

Table 2 Testing sequence and peak acceleration of input motion ($a_{peak,Input}$ [g]) in reference tests and in tests with two structures

Test	Ref.S1	Ref.S2	B-Dist.	0.5B-Dist.	0.03B-Dist.
Testing sequence	(1)	(2)	(3)	(4)	(5)
L_Input	0.086	0.088	0.091	0.092	0.094
M_Input	0.176	0.173	0.182	0.181	0.177
H_Input	0.291	0.295	0.303	0.301	0.305

2.2 Description of centrifugal test matrix

A total of five centrifuge tests were performed in this study. Reference responses of two structures were obtained by performing pair of tests named Ref.S1 and Ref.S2 after the installation of single S1 or S2 structure on ground, respectively. Fig. 3 shows the experimental layouts comprising of the S1 and S2 structures at three distance ranges from each other. Table 2 shows the testing sequence following Fig. 3 with three tests included S1 and S2 located at three distances were performed after the two reference tests. To investigate the SSSI effects, three tests were performed with the configuration layout of the two structures in three distance ranges: B, 0.5B, and 0.03B where B is the width of foundation in shaking direction. The maximum distance of B was chosen for two reasons: (1) to elicit SSSI effects; and (2) in consideration of the size of foundations and the ESB box. Note that the soil surface was carefully flattened, and structures were relocated to a new position after each test.

2.3 Earthquake input excitation

An artificial earthquake which has a high intensity and wide bandwidth frequency was applied as an input excitation. Frequency component of the input motion was filtered in the range of 40 Hz to 300 Hz before applying it to the earthquake simulator. Fig. 4 presents applied input motion both in time and frequency domains which ranges from 1 to 6 Hz in the prototype scale. To explore effects of input intensity on the structure response and SSSI, the input motion was scaled into three levels of peak acceleration (a_{peak}) as approximately 0.3 g, 0.2 g, and 0.1 g, with the names H_Input, M_Input, and L_Input, respectively. Table 2 indicates peak acceleration of input motion in reference tests (Ref.) and in tests with two structures at three distances that shows a slight difference in input peak acceleration between various tests.

2.4 Sensors implementation and data processing

Accelerometers (PCB353B17 Piezotronics) were installed into the soil, attached on ESB, horizontally and vertically bonded on the foundation and roof of the structures. A band-pass filter with a frequency range of 0.5

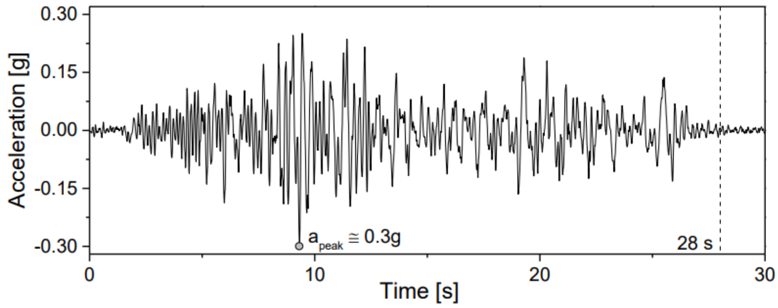

(a)

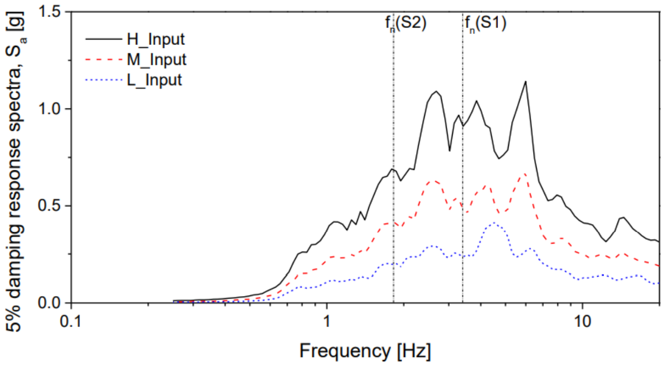

(b)

Fig. 4 Input excitation in (a) time domain; and (b) 5% pseudo response spectra. $f_n(S1)$ and $f_n(S2)$ denote fixed-base frequency of S1 and S2 structures, respectively

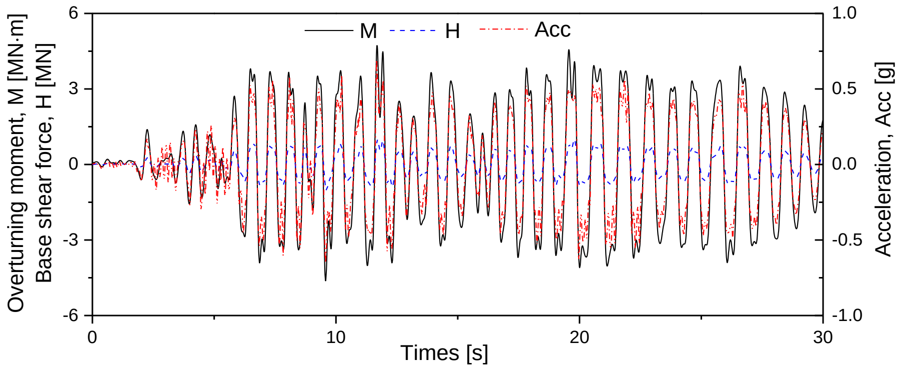

(a)

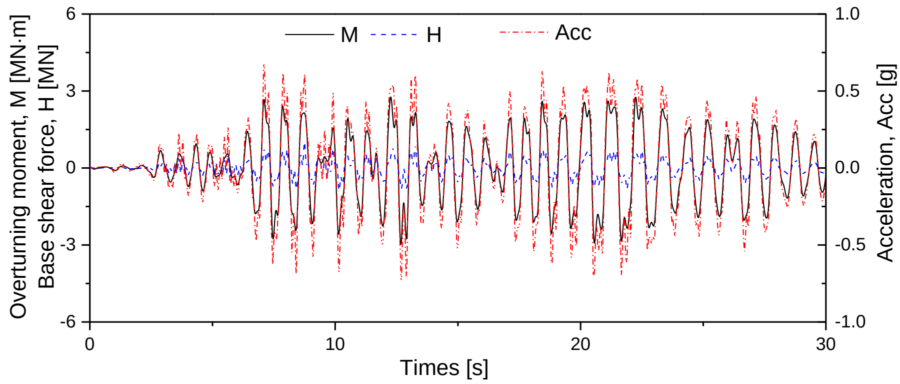

(b)

Fig. 5 Overturning moment (M), foundation base shear force (H), and roof acceleration (Acc) at H_Input level of (a) S1 and (b) S2 structures in reference tests

and 20 Hz was used to remove unrealistic frequency contents and noises in measured acceleration data. A base-line correlation algorithm was used before performing a double integration to obtain displacements and settlements

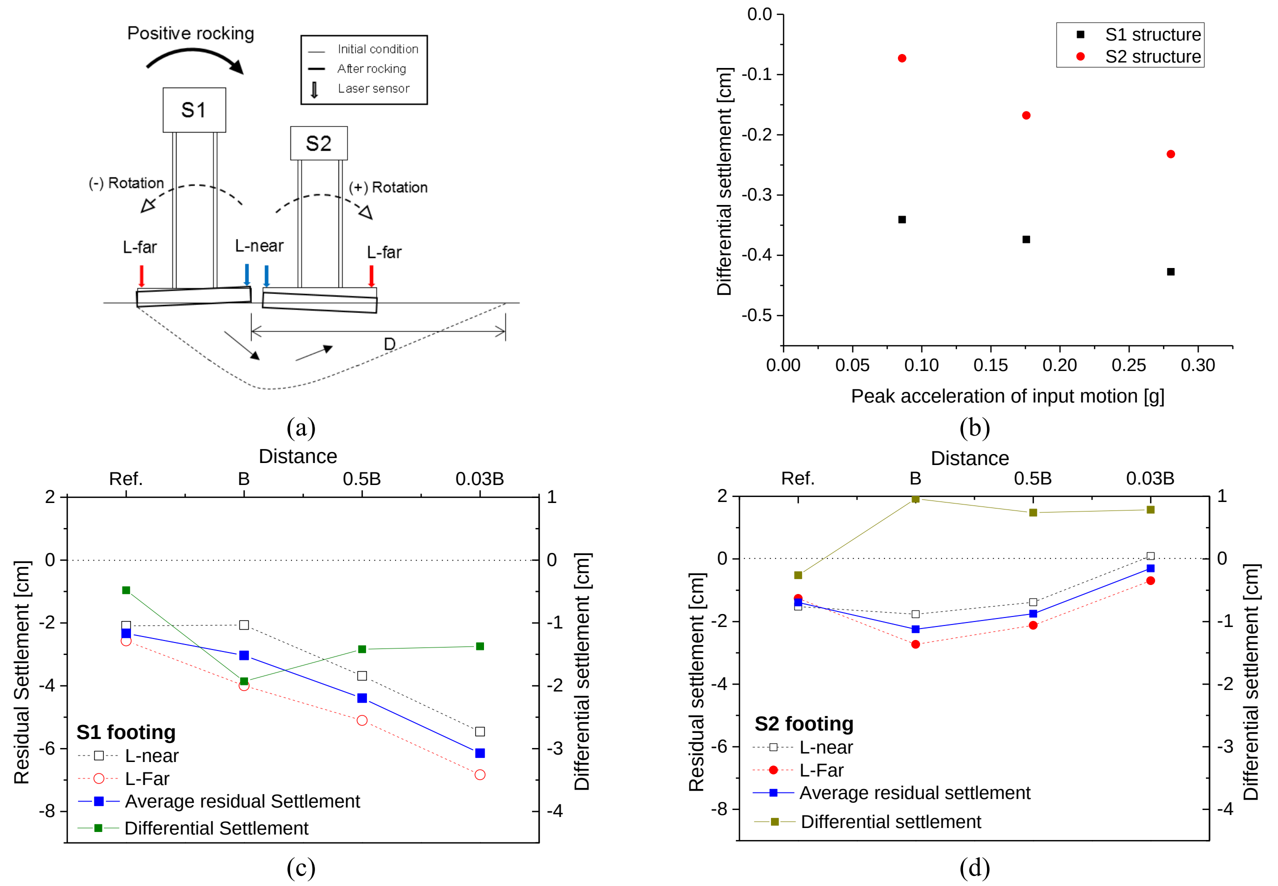

Fig. 6 Residual settlement and differential settlement: (a) sign convention and slip surface; (b) differential settlement of S1 and S2 structures at reference tests; (c) residual settlement of S1; and (d) residual settlement of S2

of the soil surface and structures from acceleration data during a seismic response. Furthermore, three pairs of strain gauges were also attached on each wall of each structure to estimate the bending strain when the input motion was applied. The locations to which strain gauges were attached were chosen at the bottom, middle, and top of the wall of each structure to define dynamic bending diagrams with three measured positions (i.e., M_top, M_mid, and M_bottom). A low-pass filter with a corner frequency of 4.5 Hz was used to remove the high-frequency noise in measured strain (Trombetta *et al.* 2013). The overturning moment (M) and foundation shear force (H) were estimated using measurements from both the strain gauges and the accelerometers by following procedures proposed by Trombetta *et al.* (2013). Firstly, dynamic wall bending diagrams were defined and drawn with the height of wall as shown in Fig. 5 with H_Input level of excitation by calculating the bending moments at three locations on the wall. Although the highest level of input excitation was applied, the linear elastic behavior of structural wall under repeated shaking could be confirmed by the linear bending moment diagram obtained. Dynamic wall shear force (H_wall) was then estimated as a slope of linear wall moment diagram in time domain. The overturning moment at the foundation was calculated by adding the moment components contributed by H_wall and by rotational inertia of the footing into the M_bottom. Finally, dynamic base shear force was calculated by adding the foundation inertia force induced by horizontal acceleration of the foundation to the H_wall. M and H were displayed in the same phase with the roof motion (RM) of each structure as indicated in Fig. 5 which implied that foundation base forces mainly induced by motion and movement of the roof.

3. Experimental results and discussion

3.1 Foundation Responses in SSSI of Couple Structures

3.1.1 Final settlement and rocking of foundations in SSSI

Fig. 6(a) shows a sign convention of rotation angle for the S1 and S2 structures. The legend markings “near” and “far” indicate the measurement of settlement depending on whether the measured position is near or far from the neighboring structures. Fig. 6(b) presents variation of differential settlement of S1 and S2 structures with input levels at reference tests. Figs. 6(c)-(d) show the residual and differential settlement of S1 and S2 structures after H_Input excitation. Note that the settlement for each structure was calculated by subtracting the measured free-field surface settlement from the measured foundation settlement. Relatively small value of differential settlement was observed for both structures in reference tests. The average settlement of the S2 structure was less than that of the S1

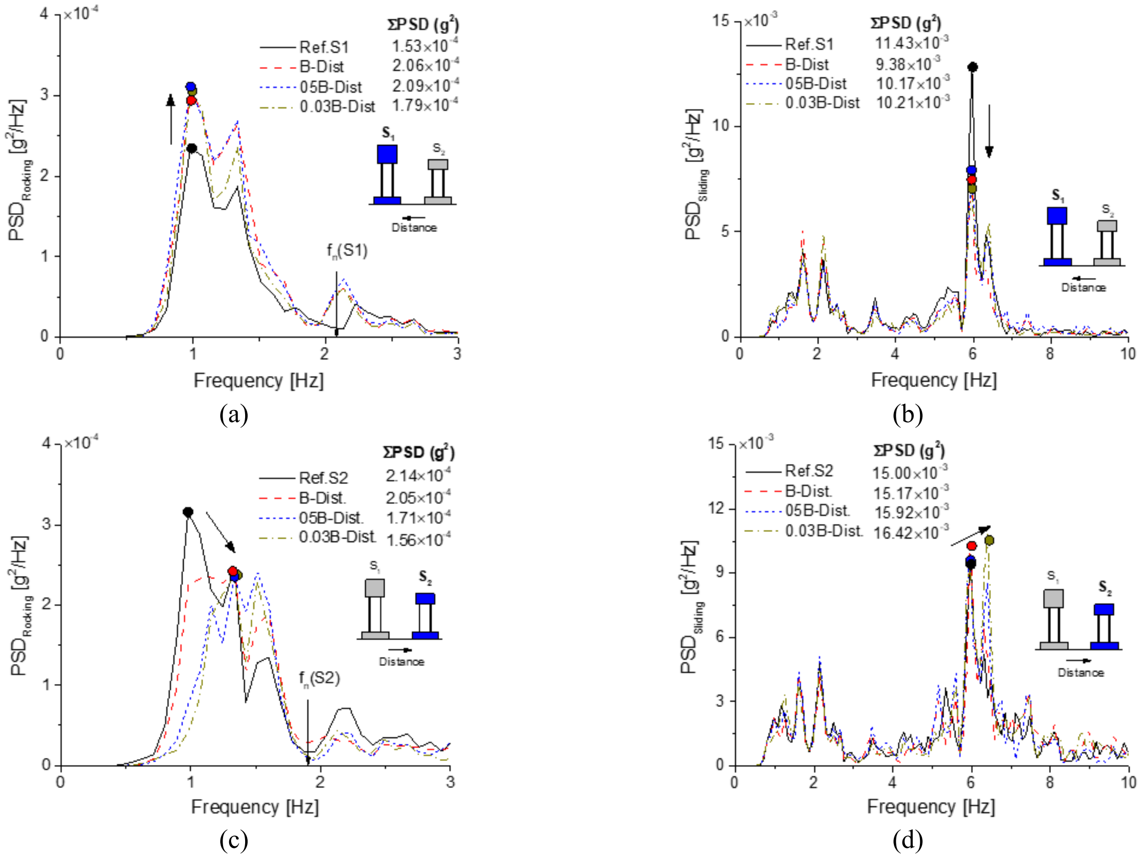

Fig. 7 Comparison of PSD of response of S1 foundation with (a) rocking and (b) sliding, and of S2 foundation with (c) rocking and (d) sliding at H_Input earthquake

structure in the reference tests because S2 has higher FS_V value than the S1 structure. When the S1 and S2 structures approached each other, the S1 structure settled more, regardless of the distance between the two structures, while the settlement of the S2 varied with distances between two structures. An uplift was experienced at the "near-side" foundation of the S2 structure at the closest distance to S1 structure (Fig. 6(d)) because horizontal movement of dense soil beneath the heavier structure (S1) to the region beneath the lighter structure (S2) and restriction from heavier S1 structure. The horizontal movement and restriction could result in the increase in differential settlement and the outward rotation of S2 from the S1 structure in SSSI as shown in Figs. 6(c)-6(d) (Knappett *et al.* 2015). The near-side foundations settled more than those in the far-side, which caused the two structures to rotate out of positions parallel to each other so that differential settlement of both structures increased when they were located near each other compared to those in reference test.

A slip surface of S1 foundation could be plotted as shown in Fig. 6(a) with expecting horizontal movement of soil beneath S1 foundation to S2 foundation and the increase in differential settlement of the S2 structure could be attributed to an assumed general shear failure of S1 structure. Distance (D) from S1 foundation to edge of slip surface was estimated based on Meyerhof's method (Meyerhof 1951) with foundation width (B) and soil friction angle (ϕ). The slip surface overlapped with the adjacent structure at any tested distances between two structures because D was approximately calculated to be 6B, which probably resulted in a slight change in differential settlements of two structures with a closer distance between two structures. Although a rocking restriction could increase the differential settlement with decreasing distance between two structures, the overlapped slip surface from adjacent structure was presumed to be one of the reasons for the observed reduction in differential settlement of both structures.

3.1.2 Rocking and slide responses of foundations and SSSI effects

The rocking motion of foundation in time domain can be defined as the ratio of difference between two vertical accelerations installed at foundation to the foundation width (B). The sliding response of foundation was obtained by subtracting horizontal free-field acceleration from horizontal foundation response. To illustrate the change in responses of structures, the power spectra density (PSD) of rocking and sliding motion were estimated with 1024-points hamming window and Welch's method (Welch 1967) as:

$$PSD_f = \frac{1}{K}\sum_{k=1}^{K} P_m(f) \tag{4}$$

where K is the number of segments, k is the order of segment, and $P_m(f)$ is modified periodogram value that $P_m(f)$ can be defined from discrete Fourier transform of each segment as:

$$P_m(f) = \frac{1}{\sum_{m=0}^{M} \omega^2(m)} |X_k(f)|^2 \quad (5)$$

where M is the number of points in each segment, $X_k(f)$ is windowed discrete Fourier transform, and $\omega(m)$ is window function.

Fig. 7 illustrates PSD of rocking and sliding response of S1 and S2 foundations in reference tests and in test with two structures at H_Input excitation. Solid points indicate the maximum value of PSD (Max.PSD). At reference tests, rocking motion of S1 foundation was amplified at around 1 Hz as shown in Figs. 7(a), while sliding response at 6 Hz (Figs. 7(b)), which are similar to theoretical rocking (f_R) and sliding (f_S) natural frequencies of the structure previously defined in Fig. 2. Moreover, the results for the reference test were compared with those in the tests regarding the S1 and S2 structures to explore the SSSI effects. It could be seen that rocking response of S1 structure increased while its sliding response decreased when S2 structure was located besides, regardless of distances between the two structures. S1 structure tended to rock than slide. The reduction in sliding response of S1 (Fig. 7(b)) structure in SSSI could be because a less massive and lower structure, S2, appeared nearby (Aldaikh *et al.* 2016; Alexander *et al.* 2013; Ogut 2017). And the reduction in sliding response under SSSI effects could probably resulted in an increase in rocking response of S1 structure because the round surface formed beneath S1 foundation when there was less horizontal movement from structure. Also, heedless of distance between two structures, frequencies at which rocking and sliding PSD of S1 structure reach maximum value were equal to those in the reference test. As a result of the proximity to the S2 structure, which is a lighter and lower one, SSSI effects did not show frequency shift both for rocking and sliding responses of the S1 structure.

In addition, inverse effects of SSSI on the rocking and sliding behaviors were observed for the S2 structure: (1) it tended to slide more than rock, and (2) both rocking and sliding frequencies of S2 structure slightly increase when S1 structure is located nearby. Because S1 structure is more massive compared to S2 structure, SSSI effects from S1 structure increased sliding response and frequencies of S2 structure during an earthquake, which was also reported by Behnamfar and Sugimura (1999) and Xu *et al.* (2004). The high rocking restriction by S1 structure and the increase in confining pressure of the soil under S2 structure due to the appearance of a more massive S1 structure caused the increase in rocking and sliding natural frequencies of S2 structure, which was not observed in the former.

Total power spectral density (ΣPSD) was estimated for PSD of rocking and sliding response of S1 and S2 structure, which is a more robust observation of change in response (Alexander *et al.* 2013). Values of ΣPSD for rocking and sliding responses of both structures at H_Input are indicated in Fig. 7. Variation in ΣPSD of each structure (ΔPSD) either for rocking or sliding response in SSSI tests (ΣPSD(SSSI)) with that in reference tests (ΣPSD(Ref)) was calculated so to estimate SSSI effects as:

$$\Delta\text{PSD}\ [\%] = \frac{\Sigma\text{PSD(SSSI)} - \Sigma\text{PSD(Ref)}}{\Sigma\text{PSD(Ref)}} \times 100 \quad (6)$$

Table 3 ΔPSD values for rocking and sliding response of S1 and S2 structures in tests with the two structures adjacent to another. Negative value in table denotes SSSI effects reduce ΣPSD of rocking or sliding response

ΔPSD (%)	$\Delta PSD_{Rocking}$ (%)			$\Delta PSD_{Sliding}$ (%)		
	L_Input	M_Input	H_Input	L_Input	M_Input	H_Input
S1 foundation						
B-Dist	46.05	43.95	35.26	-28.16	-27.98	-17.96
0.5B-Dist	45.35	39.27	37.14	-21.26	-19.09	-11.05
0.03B-Dist	34.00	24.51	17.64	-17.74	-14.19	-10.07
S2 foundation						
B-Dist	-10.81	-8.05	-6.09	7.19	2.14	1.15
0.5B-Dist	-26.08	-34.51	-22.10	32.33	26.67	6.13
0.03B-Dist	-42.74	-37.05	-38.39	43.06	45.31	9.52

Table 3 listed the ΔPSD values of S1 and S2 structure as regards to the rocking and sliding responses at three levels of input excitation. A negative value of ΔPSD indicates that SSSI effects reduce total rocking or sliding response of structure. SSSI effects increased $\Sigma PSD_{rocking}$ and decreased $\Sigma PSD_{sliding}$ of S1 structure, while it reduced rocking response and increased sliding response of S2 structure when they were located adjacent to each other, regardless of input excitation level. As input intensity increased, the less extreme change in ΣPSD of rocking and sliding response for two structures implied that SSSI effects on rocking and sliding motions of foundation reduced at a higher intensity of earthquake. The reduction in stiffness of soil-structure system with increasing input level could have resulted in the decrease of SSSI effects with earthquake intensity (Ha *et al.* 2014, Seong *et al.* 2017). Furthermore, as distance between two structure decreased (i.e., from B to 0.03B), $\Delta PSD_{rocking}$ of S1 and S2 structures decreased and $\Delta PSD_{sliding}$ increased. In this study, restriction by adjacent structures increased with decreasing distance between two structures and the wave emitted from nearby structures probably increased $\Delta PSD_{sliding}$ in both structures (Alexander *et al.* 2013, Padrón *et al.* 2009). Moreover, the overlap of slip surface to adjacent structure during rocking and the increase in sliding response for both structures with reduction in distance between two structures could resulted in the decrease in rocking response and the differential settlement as shown in Figs. 6(c) and 6(d) because the soil beneath structures could be flattened during sliding of the structure.

3.2 Foundation force demands

3.2.1 Foundation shear force and overturning moment

In geotechnical engineering and foundation design, it is very important to estimate the forces applied to foundation, including base shear force and overturning moment during an earthquake. However, there is less information on how the foundation forces of a target structure are modified by an adjacent foundation. During an earthquake loading, the foundation base shear force (H) is induced by the inertia

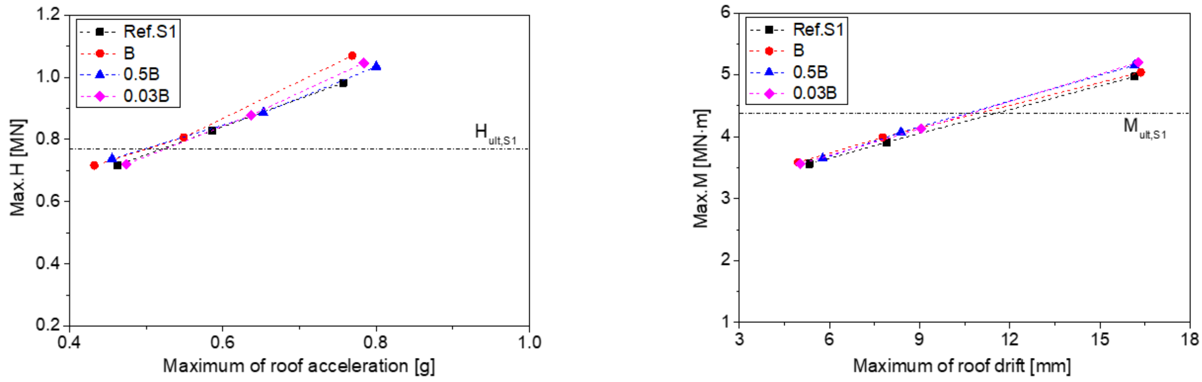

(a) (b)

Fig. 8 (a) Maximum foundation base shear (Max.H) vs. maximum roof acceleration; and (b) Maximum overturning moment (Max.M) vs. maximum roof drift of S1 structure

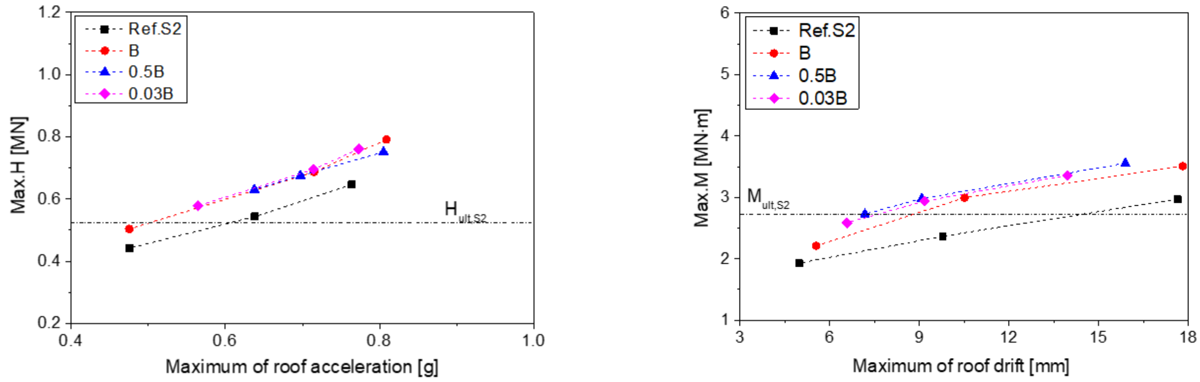

(a) (b)

Fig. 9 (a) Maximum foundation base shear (Max.H) vs. maximum roof acceleration; and (b) Maximum overturning moment (Max.M) vs. maximum roof drift of S2 structure

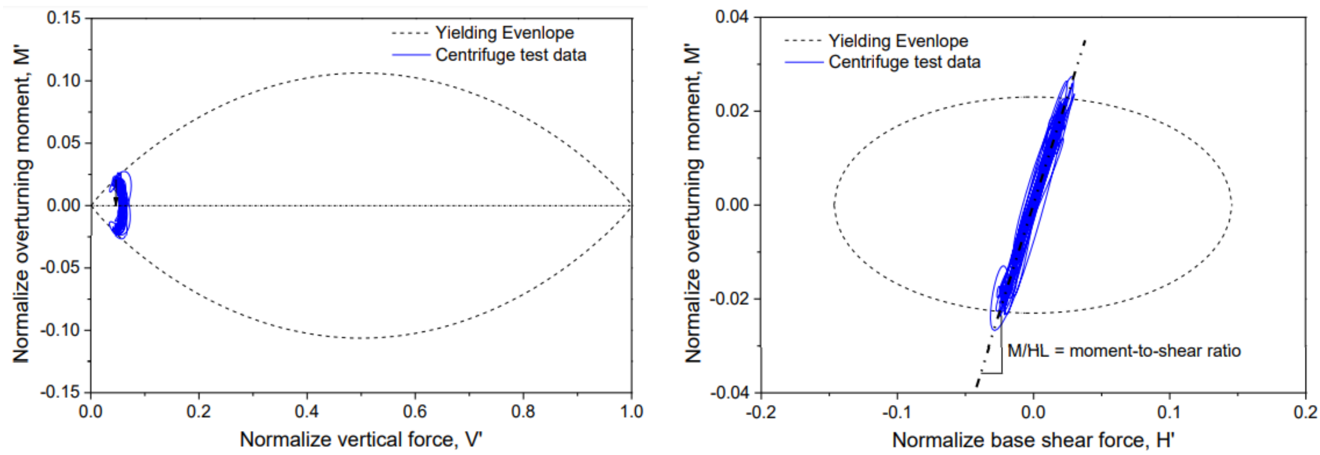

(a) (b)

Fig. 10 Normalized H-V-M bounding surface and earthquake loading path in (a) M-V plane; and (b) M-H plane for S1 structure in reference test at H_Input

acceleration of the structure, as illustrated in Fig. 5, while the rocking and overturning moment (M) is mainly related to the horizontal deformation of the roof of a structure (Trombetta *et al.* 2013).

Figs. 8 and 9 present the relationship between maximum base shear force (Max.H) and peak acceleration of the roof and the relationship between maximum overturning moment (Max.M) and maximum roof drift for both structures at three levels of input excitation (i.e., L_Input, M_Input, and H_Input), respectively. The roof drift was calculated by subtracting horizontal movement of soil free-field from total roof translation. Note that in Figs. 8-9, the ultimate base shear force (H_{ult}) and ultimate overturning moment (M_{ult}) for each structure were also plotted. The ultimate overturning moment (M_{ult} = W_p·L(1-1/FS_v)/2) where L is length of the foundation) was determined from the total weight of the structures (W_p) and the vertical safety factor (FS_V). The ultimate base shear force (H_{ult}= μ·W_p) was defined based on the value of W_p and the friction coefficient (μ) between the soil and the foundation (Gazetas *et al.* 2014). For both structures, it was observed that a linear increase in H and M in reference tests and in tests including two structures with peaks of structure drift and acceleration, respectively. Regardless of input excitation level, the S1 structure experienced much higher values of both H and M than the S2 structure, probably because of high H_{ult} and M_{ult} values of S1 structure. Moreover, maximum values of H and M under the largest input excitation (i.e., H_Input) were estimated to be larger than H_{ult} and M_{ult}, respectively, due to the damping effects of the rocking and sliding responses (Kim *et al.* 2015).

SSSI effects can be revealed by comparing the relationships between Max.H and Max.M with maximum structure acceleration and roof drift obtained in the reference tests to those in tests with the two structures (Trombetta *et al.* 2013). As shown in Fig. 8, Max.H and Max.M of S1 structure under SSSI effects (i.e., B, 0.5B, and 0.03B cases with S2) were slightly larger than in the reference test at H_Input input motion. In addition, SSSI effects on H and M were evaluated for the S2 structure when it was adjacent to the larger S1 structure, as shown in Fig. 9. Compared to results in reference test, both Max.H and Max.M of the S2 structure significantly increased in test with adjacent S1 structure, which indicates that H_{ult} and M_{ult} values of the S2 structure were enlarged. This behavior was not observed in the S1 structure because it was much larger than the S2. Therefore, S1 imposed more restriction on the S2 structure during an earthquake when they were built close to each other (Trombetta *et al.* 2014). The distance effects can be more clearly observed in relationship between M and roof acceleration of S2 structure as shown in Fig. 9(b). As the distance between the two structures decreased, M_{ult} of the S2 structure increased, and it approaches the peak at the closest distance. An increase in rocking restriction with a reduction in the distance between two structures under SSSI effects, which is indicated by a decrease in the rocking response (Fig. 7(c) and Table 3), could be one of the reasons for the increase in M_{ult} of S2 structure (Aldaikh *et al.* 2016; Alexander *et al.* 2013).

3.2.2 Combined V-H-M footing loading and yielding envelope

In addition to the base shear force (H) and the overturning moment (M) at the soil-foundation interface, the vertical force (V) is applied by the structure weight and vertical acceleration, which causes a coupling V-H-M effect during an earthquake acceleration. The yielding envelope for a foundation located on the ground in V-H-M loading spaces proposed by Cremer *et al.* (2001) has a parabolic shape in the V-H and V-M plane and an elliptical section in the M-H plane as:

$$\left(\frac{H'}{aV'^{c}(1-V')^{d}}\right)^{2}+\left(\frac{M'}{bV'^{e}(1-V')^{f}}\right)^{2}-1=0 \quad (7)$$

Table 4 Moment-to-shear ratio (M/HL) of S1 and S2 structures in reference tests and in SSSI tests at various distances

Test	S1			S2		
	L_Input	M_Input	H_Input	L_Input	M_Input	H_Input
Ref.	0.880	0.877	0.876	0.8408	0.8407	0.840
B-Dist	0.893	0.892	0.884	0.830	0.826	0.822
0.5B-Dist	0.890	0.889	0.886	0.826	0.825	0.823
0.03B-Dist	0.888	0.887	0.884	0.828	0.822	0.821

where V', H', and M' are obtained by normalizing as follows: V' = V/V_{ult}, H' = H/V_{ult}, and M' = M/ V_{ult}·L with V_{ult} is ultimate bearing capacity of structure. *a*, *b*, *c*, *d*, *e*, and *f* are shape parameters in M-H, H-V, and M-V planes and those were defined by Trombetta *et al.* (2014) for dense sand ground.

Fig. 10 shows the experimentally measured earthquake loading path in M-V and M-H planes for the S1 structure at high input intensity (H_Input) with the yielding envelopes plotted as dotted-line. As the vertical load decreased, the overturning moment and base shear force increased. The loading path reaches and follows the yielding envelope which implies a reduction in both M and V until the next earthquake arrives. With a yielding point in the V' plane of approximately 0.045 (the arrow in Fig. 10(a)), the yielding envelope in the M-H plane was defined by Eq.(7) and plotted in Fig. 10(b). Similar results were obtained for reference test with S2 structure.

The loading path in the M-H plane could be considered as a straight line with its slope as the moment-to-shear ratio, M/(H·L), (Fig. 10(b)). M/(H·L) ratio is a key parameter that decides the rocking and sliding behaviors of a structure during an earthquake (Gajan and Kutter 2009b). Modification of the estimated M/(H·L) value for the S1 and S2 structures due to the presence of an adjacent structure are listed in Table 4. In reference tests, the M/(H·L) ratio for the S1 structure was higher than that observed in S2 at all input levels because S1 was higher and has a heavier top mass than the other. A slight change in M/(H·L) value could be detected when the two structures were located close to each other: the M/(H·L) ratio of the S2 structure decreased slightly, while that of the S1 structure increased, implying that S1 structure tended to rotate, and the S2 structure tended to slide in SSSI phenomena (Gajan and Kutter 2009b). This observation supports the results in Fig. 7, which shows that the rocking response of S1 and the sliding motion of S2 increased more than that of the reference tests. Moreover, as the distance between structures decreased (i.e., from B to 0.03B), the M/(H·L) ratio of S1 and S2 structures slightly decreased. These decrements indicate that both structures tended to slide more when their distance decreased, which were observed in Fig. 7 and Table 3.

3.3 Nonlinear rocking and sliding responses of foundation under SFSI and SSSI effects

The base forces and deformation of the foundation both in the reference tests and in the tests with the two structures have been discussed earlier. In this section, more attention will be paid to coupled load-deformation behaviors of the foundations, which are illustrated by moment-rotation and base-shear force-slide loops. Fig. 11 presents normalized moment–rotation (M/M_{ult}-θ) and normalized base-shear force–horizontal slide (H/H_{ult}-δ) responses at medium (M_Input) and high (H_Input) input intensity for the S1 and S2 foundations, respectively. Dash-dot lines at unity in Fig. 11 indicate M_{ult} and H_{ult} of each structure. It was observed that a nonlinear increase in the rocking and sliding angle of S1 and S2 structures as M and H increased, until the ultimate values (i.e., M_{ult} and H_{ult}) were reached. After that, M and H decreased with increasing rocking angle and sliding amplitude which indicates M and H followed the yielding envelope as mentioned above. Backbone curves were plotted by estimating nonlinear rocking (k_θ) and sliding stiffness (k_δ) as following steps. Rocking secant stiffness can be defined as ratio of the maximum overturning moment and rocking angle ($k_\theta = M/\theta$), while slide stiffness is the slope of H-δ response at the extreme point of each hysteretic loop (Cremer *et al.* 2001, Kim *et al.* 2015) in Fig. 11. The calculated k_θ and k_δ were normalized to the theoretical maximum rocking stiffness ($k_{\theta,Max}$) and sliding stiffness ($k_{\delta,Max}$), which were calculated from the initial shear modulus of soil beneath structure (G_{max}), moment of inertia at centroid of the foundation in the direction of rocking (I), and foundation dimensions (i.e., length of L and width of B) as (Gazetas 1991):

$$k_{\theta,Max} = \frac{G_{max}}{1-\vartheta} I^{0.75} \left(\frac{L}{B}\right)^{0.25} \left[2.4 + 0.5\frac{B}{L}\right] \ (\mathrm{KN \cdot m}) \quad (8)$$

$$k_{\delta,Max} = \frac{G_{max} L}{2-\vartheta}(2 + 2.5 \cdot 0.25^{0.85}) \ (\mathrm{KN/m}) \quad (9)$$

where G_{max} could be defined as 2.5 times of the initial shear modulus at the free-field ($G_{max}^{free\text{-}field}$) because of the high confining stresses below the foundations (Trombetta *et al.* 2014). Fig. 12 shows the normalized rocking stiffness, $k_\theta/k_{\theta,Max}$ and sliding stiffness $k_\delta/k_{\delta,Max}$ of the S1 and S2 structures at all three input intensities. For normalized rocking stiffness (Fig. 12 in the left), there were two groups of data: loading stage and free-rocking stage. Data for the loading stage, which is displayed as rectangular points, were extracted from M~θ loops before 28 seconds in time domain or in the seismic. Data for the free-rocking stage (i.e., structure rotated by its vibration where there was no applied input acceleration as indicated in Fig. 4) plotted as circular points were obtained after 28 seconds. In the free-rocking stage, the rocking stiffness was smaller than that in the loading stages in both structures because rounding curves of soil surface beneath foundations were formed when they rotated during the loading stage, which reduced the rocking stiffness (Gajan and Kutter 2008). The rocking and sliding stiffness of the two structures decreased with an increase in rocking angle and sliding deformation because the contact area between foundations and soil drastically decreased (Gajan and Kutter 2009a). A power function of normalized rocking stiffness to the rocking angle (θ) (Gajan *et al.* 2005) was implemented to illustrate degradation of k_θ. It was modified in the form of Eq. (10) and was also used for normalized sliding stiffness ($k_\delta/k_{\delta,Max}$) with respect to horizontal slide δ (m) as:

$$\frac{k_\theta}{k_{\theta,Max}} \ or \ \frac{k_\delta}{k_{\delta,Max}} = A(\theta^B) \ or \ C(\delta^D) \quad (10)$$

where A and B or C and D are the fitting parameters of the degradation function defined from tested data with the single S1 or S2 structures, respectively, with regression values over 0.9. A and C indicate values of $k_\theta/k_{\theta,Max}$ and $k_\delta/k_{\delta,Max}$ at amplitudes of θ and δ is one; while B and D values show increase of k_θ and k_δ with a decrease in θ and δ. Estimated backbone curves were plotted in the Fig. 11 with the corresponding A, B, C, and D values. Value of A for S1 structure (A_{S1} = 0.0018) was lower than that for S2 structure (A_{S2} = 0.0063) because S1 structure is more massive and higher than S2, and also the aspect ratio (h_{eff}/r_θ value in Table 1) of S1 structure is higher than S2 structure, which results in S1 structure rotated more than S2. However, S1 structure show a higher value of $k_\theta/k_{\theta,Max}$ at a small rocking angle compared to that in S2 structure (B_{S1} was smaller than B_{S2}) because S1 structure has a higher value of rocking equivalent foundation radius (i.e., r_θ in Fig. 2), that could lead to higher rocking resistance at low amplitude earthquake. The larger sliding equivalent foundation radius (i.e., r_e value in Fig. 2) of S1 structure also lead to larger normalized sliding stiffness (i.e., S1 structure has slightly larger value of C and lower value of D as shown in Fig. 12) relatively compared to those observed for S2.

In this study, rocking and sliding responses of the S1 and S2 structures were observed when two structures were located at various distances to another (i.e., B, 0.5B, and 0.03B). By determining the rocking and sliding stiffness of the S1 and S2 foundations, SSSI effects can be known. Fig. 13 shows variations in rocking and sliding stiffness of the S1 and S2 structures at various distances between them at all three input intensities. Lines of best fit with power function were obtained for both structures at all tests, with regression values of over 0.89. Regardless of distances between S1 and S2 structures, rocking stiffness of S1 structure decreased while its sliding stiffness increased when compared to those in reference tests (Figs. 13(a)). The decrease in rocking stiffness and increase in sliding stiffness were more noticeable at small values of θ and δ, which signifies that SSSI effects are notable during a low intensity earthquake that coincides with results of ΔPSD observed in Table 3 both for rocking and sliding responses. The reduction in the rocking stiffness and the increase in the sliding stiffness illustrates the tendency of rocking rather than sliding of S1 structure due to SSSI effects as observed in Figs. 7(a)-(b). Reduction in the distance between the two structures seems to slightly increase the rocking stiffness of the S1 structure due to the reduction in rocking response (Table 3). Sliding stiffness of S1 structure at large value of δ slightly decreased with a decrease in distance between structures because its sliding response slightly increased at a closer distance between structures as shown in Fig. 7(b). In contrast to response of the S1 structure under SSSI effects, a lesser rocking behavior in the S2 structure was observed (Fig. 7(c)) resulting in an increase in the rocking stiffness (Fig. 13(c)), while sliding stiffness remained the same (Fig. 13(d)). The sliding stiffness in S2 structure was unchanged probably due to the fact that both sliding response and base shear force (H) increased compared to the reference test as shown in Figs. 7(d) and 9(a), respectively. As the distance

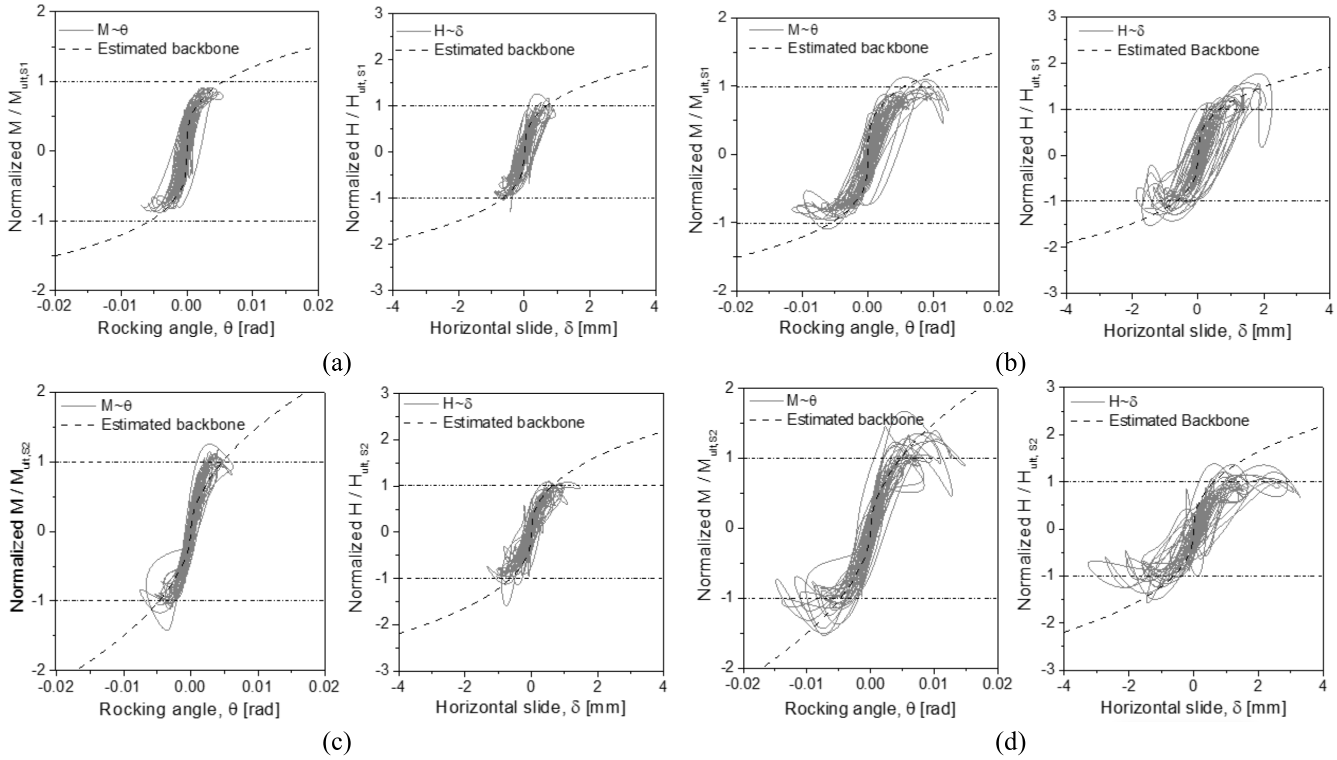

Fig. 11 Overturning moment–rocking angle and base shear force–slide responses in test of (a) S1 structure at M_Input, (b) S1 structure at H_Input, (c) S2 structure at M_Input and (d) S2 structure at H_Input

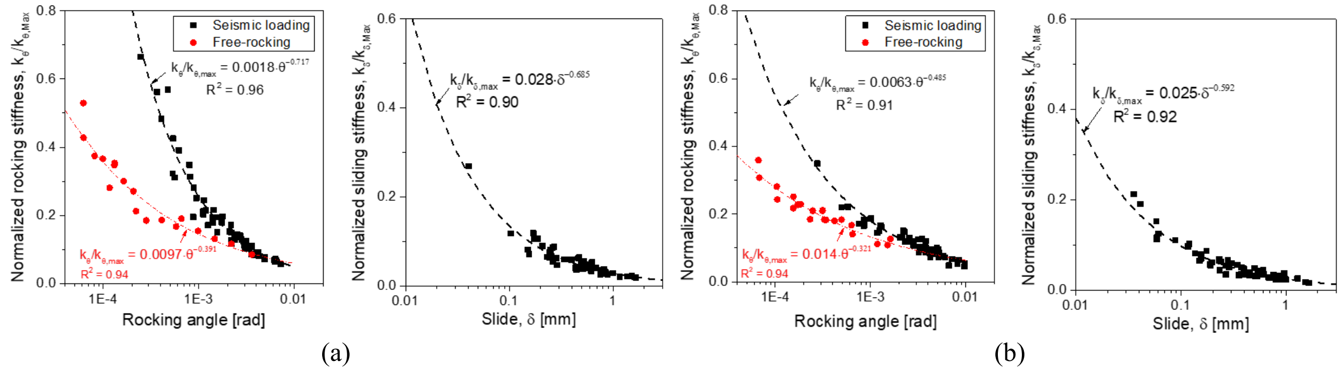

Fig. 12 Power degradation of rocking and sliding stiffness with rocking angle and slide for (a) S1 structure; and (b) S2 structure, respectively

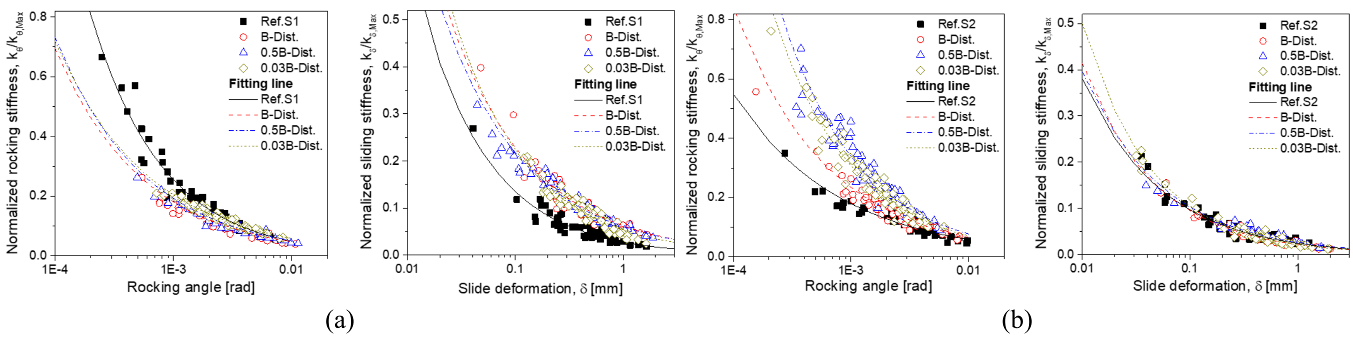

Fig. 13 Comparison of normalized rocking and sliding stiffness with rocking angle and slide deformation for (a) S1 structure; and (b) S2 structure, respectively

between the two structures decreased, the rocking stiffness of the S2 structure increased because of the decrease in rocking response of the S2 structure as depicted in Fig. 7(c).

Both sliding response and base shear force (H) increased with reduction in distance between structure which causes the steadiness in observed sliding stiffness of the S2 structure.

4. Conclusions

Five centrifuge tests were performed to investigate SFSI and SSSI effects on two structures. Three dynamic geo-centrifuge tests composed of two structures were performed, and the results were compared to reference responses obtained by two test series on each of the structures. The main findings are as follows:

1. SSSI effects caused a more residual settlement and differential for the larger structure (S1) regardless of distance between two structure. However, the small structure (S2) settled down more at B distance between the two structures, and less settlement with an uplift at near side foundation was observed at a closer distance between the two structures, which results in S2 structure rotating out of S1 structure after the test. Differential settlement of the two structures slightly changed with variations in distance between two structures due to overlap of slip surface from adjacent structure.

2. SSSI have different effects on rocking and sliding responses as well as foundation base forces of the two structures:

a) For the smaller structure (S2) interacting with the larger structure (S1): small structure tends to slide more and rock less because there was an increase in $PSD_{sliding}$ and a reduction in $PSD_{rocking}$ in SSSI tests. These results were also contributed by a slight decrease in the moment-to-shear ratio (M/(H·L)), regardless the distance between the two structures. A decrease in distance between two structures resulted in a less rocking and a more sliding responses of S2 structure because the increase in rocking restriction and wave emitted from adjacent and vibrating structure. Restriction causes a great increase in foundation base forces in smaller structure including base shear (H) and overturning moment (M), which gave rise to a significant increase in ultimate foundation base forces (i.e., M_{ult} and H_{ult}).

b) For the larger structure (S1) interacting with the smaller structure (S2): large structure tends to rock more than slide, which was indicated by an increase in the $PSD_{rocking}$ and reduction in $PSD_{sliding}$. The ratio of M/(H·L) in the S1 structure was increased which is the opposite of the effects on the S2 structure. As distance between the two structure decreases, slight increase in sliding and decrease in rocking responses were observed due to the transferred wave from adjacent structure.

3. A less rocking stiffness and more sliding stiffness were observed in S1 structure in SSSI tests, regardless of distance between two structures. Opposite effects on S2 structure was observed when rocking stiffness increased and sliding stiffness was similar compared to those in reference test. A decrease in distance between two structures seems to slightly increase rocking stiffness, however, slightly decreased sliding stiffness of S1 structure at high input intensity, which could be attributed to the increase in sliding response. Rocking stiffness of S2 structure was increased with a decrease in distance from S1 structure due to the reduction in rocking response of S2 structure and the rise in rocking restriction from larger structure.

Acknowledgments

This research was supported by the National Research Foundation of Korea (NRF) grant funded by the Korean government (NRF-2017R1C1B2004036) and by the Korea Institute of Energy Technology Evaluation and Planning (KETEP) and the Ministry of Trade, Industry & Energy (MOTIE) of the Republic of Korea (No. 20161520101130).

References

Aldaikh, H., Alexander Nicholas, A., Ibraim, E. and Knappett Jonathan, A. (2018), "Evaluation of rocking and coupling rotational linear stiffness coefficients of adjacent foundations", *Int. J. Geomech.*, **18**(1), 04017131. https://doi.org/10.1061/(ASCE)GM.1943-5622.0001041.

Aldaikh, H., Alexander, N. A., Ibraim, E. and Oddbjornsson, O. (2015), "Two dimensional numerical and experimental models for the study of structure–soil–structure interaction involving three buildings", *Comput. Struct.*, **150**(Supplement C), 79-91 .https://doi.org/10.1016/j.compstruc.2015.01.003

Aldaikh, H., Alexander, N. A., Ibraim, E. and Knappett, J. (2016), "Shake table testing of the dynamic interaction between two and three adjacent buildings (SSSI)", *Soil Dyn. Earthq. Eng.*, **89**, 219-232. https://doi.org/10.1016/j.soildyn.2016.08.012.

Alexander, N. A., Ibraim, E. and Aldaikh, H. (2013), "A simple discrete model for interaction of adjacent buildings during earthquakes", *Comput. Struct.*, **124**, 1-10. https://doi.org/10.1016/j.compstruc.2012.11.012.

Anastasopoulos, I., Kourkoulis, R., Gelagoti, F. and Papadopoulos, E. (2012), "Rocking response of SDOF systems on shallow improved sand: An experimental study", *Soil Dyn. Earthq. Eng.*, **40**, 15-33. https://doi.org/10.1016/j.soildyn.2012.04.006.

ASCE (2017), *Seismic Analysis of Safety-Related Nuclear Structures (4-16)*, American Society of Civil Engineers, U.S.A.

Beards, C.F. (1996), *Structural Vibration: Analysis and Damping*, Arnold, London, U.K.

Behnamfar, F. and Sugimura, Y. (1999), "Dynamic response of adjacent structures under spatially variable seismic waves", *Prob. Eng. Mech.*, **14**(1), 33-44. https://doi.org/10.1016/S0266-8920(98)00033-2.

Chen, J.C., Masienikov, O.R. and Johnson, J.J. (1997), "Seismic response of a nuclear power generation complex including structure-to-structure interaction effects", *Proceedings of the American Society of Mechanical Engineers (ASME) Pressure Vessel and Piping Conference*, Orlando, Florida, U.S.A., January.

Cho, H.I., Sun, C.G., Kim, J.H. and Kim, D.S. (2018), "OCR evaluation of cohesionless soil in centrifuge model using shear wave velocity", *Geomech. Eng.*, **15**(4), 987-995. https://doi.org/10.12989/gae.2018.15.4.987.

Cremer, C., Pecker, A. and Davenne, L. (2001), "Cyclic macro-element for soil–structure interaction: material and geometrical non-linearities", *Int. J. Numer. Anal. Meth. Geomech.*, **25**(13), 1257-1284. https://doi.org/10.1002/nag.175.

Drosos, V., Georgarakos, T., Loli, M., Anastasopoulos, I., Zarzouras, O. and Gazetas, G. (2012), "Soil-foundation-structure interaction with mobilization of bearing capacity: Experimental study on sand", *J. Geotech. Geoenviron. Eng.*, **138**(11), 1369-1386. https://doi.org/10.1061/(ASCE)GT.1943-

5606.0000705.
Fatahi, B., Tabatabaiefar, S.H.R. and Samali, B. (2014), "Soil-structure interaction vs Site effect for seismic design of tall buildings on soft soil", *Geomech. Eng.*, **6**(3), 293-320. http://dx.doi.org/10.12989/gae.2014.6.3.293.
FEMA (2005), "Improvement of nonlinear static seismic analysis procedures", FEMA 440, prepared by Applied Technology Council (ATC-55 Project).
Gajan, S. and Kutter, B.L. (2009b), "Effects of moment-to-shear ratio on combined cyclic load-displacement behavior of shallow foundations from centrifuge experiments", *J. Geotech. Geoenviron. Eng.*, **135**(8), 1044-105. https://doi.org/10.1061/(ASCE)GT.1943-5606.0000034.
Gajan, S. and Kutter, B.L. (2008), "Capacity, settlement, and energy dissipation of shallow footings subjected to rocking", *J. Geotech. Geoenviron. Eng.*, **134**(8), 1129-1141. https://doi.org/10.1061/(ASCE)1090-0241(2008)134:8(1129).
Gajan, S. and Kutter, B.L. (2009a), "Contact interface model for shallow foundations subjected to combined cyclic loading", *J. Geotech. Geoenviron. Eng.*, **135**(3), 407-419. https://doi.org/10.1061/(ASCE)1090-0241(2009)135:3(407).
Gajan, S., Kutter, B.L., Phalen, J.D., Hutchinson, T.C. and Martin, G.R. (2005), "Centrifuge modeling of load-deformation behavior of rocking shallow foundations", *Soil Dyn. Earthq. Eng.*, **25**(7), 773-783. https://doi.org/10.1016/j.soildyn.2004.11.019.
Gazetas, G. (1991), *Foundation Vibrations*, in *Foundation Engineering Handbook*, Springer US, Boston, Massachusetts, U.S.A., 553-593.
Gazetas, G., Anastasopoulos, I. and Garini, E. (2014), "Geotechnical design with apparent seismic safety factors well-bellow 1", *Soil Dyn. Earthq. Eng.*, **57**, 37-45. https://doi.org/10.1016/j.soildyn.2013.10.002.
Gazetas, G., Anastasopoulos, I., Adamidis, O. and Kontoroupi, T. (2013), "Nonlinear rocking stiffness of foundations", *Soil Dyn. Earthq. Eng.*, **47**, 83-91. https://doi.org/10.1016/j.soildyn.2012.12.011.
Ha, J.G., Lee, S.H., Kim, D.S. and Choo, Y.W. (2014), "Simulation of soil–foundation–structure interaction of Hualien large-scale seismic test using dynamic centrifuge test", *Soil Dyn. Earthq. Eng.*, **61**(Supplement C), 176-187. https://doi.org/10.1016/j.soildyn.2014.01.008.
Kim, D.K., Lee, S.H., Kim, D.S., Choo, Y.W. and Park, H.G. (2015), "Rocking effect of a mat foundation on the earthquake response of structures", *J. Geotech. Geoenviron. Eng.*, **141**(1), 04014085. https://doi.org/10.1061/(ASCE)GT.1943-5606.0001207.
Kitada, Y., Hirotani, T. and Iguchi, M. (1999), "Models test on dynamic structure–structure interaction of nuclear power plant buildings", *Nucl. Eng. Des.*, **192**(2), 205-216. https://doi.org/10.1016/S0029-5493(99)00109-0.
Knappett, J.A., Madden, P. and Caucis, K. (2015), "Seismic structure–soil–structure interaction between pairs of adjacent building structures", *Géotechnique*, **65**(5), 429-441. https://doi.org/10.1680/geot.SIP.14.P.059.
Ko, K.W., Ha, J.G., Park, H.J. and Kim, D.S. (2018), "Soil-rounding effect on embedded rocking foundation via horizontal slow cyclic tests", *J. Geotech. Geoenviron. Eng.*, **144**(3), 04018004. https://doi.org/10.1061/(ASCE)GT.1943-5606.0001848.
Kobori, T., Minai, R. and Kusakabe, K. (1973), "Dynamical characteristics of soil-structure cross-interaction system", *Depart. Bull. Paper*, **22**(02), 111-151
Kwon, M.H. (2012), "Contact interface fiber section element: Shallow foundation modeling", *Geomech. Eng.*, **4**(3), 173-190. https://doi.org/10.12989/gae.2012.4.3.173
Lee, S.H., Choo, Y.W. and Kim, D.S. (2013), "Performance of an equivalent shear beam (ESB) model container for dynamic geotechnical centrifuge tests", *Soil Dyn. Earthq. Eng.*, **44**(Supplement C), 102-114. https://doi.org/10.1016/j.soildyn.2012.09.008.
Lee, T.H. and Wesley, D.A. (1973), "Soil-structure interaction of nuclear reactor structures considering through-soil coupling between adjacent structures", *Nucl. Eng. Des.*, **24**(3), 374-387. https://doi.org/10.1016/0029-5493(73)90007-1.
Lou, M., Wang, H., Chen, X. and Zhai, Y. (2011), "Structure-soil-structure interaction: Literature review", *Soil Dyn. Earthq. Eng.*, **31**(12), 1724-173. https://doi.org/10.1016/j.soildyn.2011.07.008.
Mason, H.B., Trombetta, N.W., Chen, Z., Bray, J.D., Hutchinson, T.C. and Kutter, B.L. (2013), "Seismic soil–foundation–structure interaction observed in geotechnical centrifuge experiments", *Soil Dyn. Earthq. Eng.*, **48**(Supplement C), 162-174. https://doi.org/10.1016/j.soildyn.2013.01.014.
Meyerhof, G.G. (1951), "The ultimate bearing capacity of foundations", *Géotechnique*, **2**(4), 301-332 https://doi.org/10.1680/geot.1951.2.4.301.
Ogut, O.C. (2017). "Soil-structure interaction effect of embedded foundation and adjacent buildings on response characteristics of superstructures", Ph.D. Thesis, Nagoya University, Nagoya, Japan.
Padrón, L.A., Aznárez, J.J. and Maeso, O. (2009), "Dynamic structure–soil–structure interaction between nearby piled buildings under seismic excitation by BEM–FEM model", *Soil Dyn. Earthq. Eng.*, **29**(6), 1084-1096. https://doi.org/10.1016/j.soildyn.2009.01.001.
Park, H.J., Ha, J.G., Kwon, S.Y., Lee, M.G. and Kim, D.S. (2017), "Investigation of the dynamic behaviour of a storage tank with different foundation types focusing on the soil-foundation-structure interactions using centrifuge model tests", *Earthq. Eng. Struct. Dyn.*, **46**(14), 2301-2316. https://doi.org/doi:10.1002/eqe.2905.
Schofield, A.N. (1980), "Cambridge geotechnical centrifuge operations", *Géotechnique*, **30**(3), 227-268. https://doi.org/10.1680/geot.1980.30.3.227.
Seong, J.T., Ha, J.G., Kim, J.H., Park, H.J. and Kim, D.S. (2017), "Centrifuge modeling to evaluate natural frequency and seismic behavior of offshore wind turbine considering SFSI", *Wind Energy*, **20**(10), 1787-1800. https://doi.org/10.1002/we.2127.
Trombetta, N.W., Mason, H.B., Chen, Z., Hutchinson, T.C., Bray, J.D. and Kutter, B.L. (2013), "Nonlinear dynamic foundation and frame structure response observed in geotechnical centrifuge experiments", *Soil Dyn. Earthq. Eng.*, **50**, 117-133. https://doi.org/10.1016/j.soildyn.2013.02.010.
Trombetta, N.W., Mason, H.B., Hutchinson, T.C., Zupan, J.D., Bray, J.D. and Kutter, B.L. (2014). "Nonlinear soil–foundation–structure and structure–soil–structure interaction: centrifuge test observations", *J. Geotech. Geoenviron. Eng.*, **140**(5), 04013057. https://doi.org/10.1061/(ASCE)GT.1943-5606.0001074.
Welch, P. (1967), "The use of fast Fourier transform for the estimation of power spectra: A method based on time averaging over short, modified periodograms", *IEEE T. Audio Electroacous.*, **15**(2), 70-73.
Xu, J., Costantino, C., Hofmayer, C. and Ali, S. (2004), "Seismic response prediction of NUPEC's field model tests of NPP structures with adjacent building effect", *Proceedings of the ASME/JSME 2004 Pressure Vessels and Piping Conference*, San Diego, California, U.S.A.

IC